Panchromatic and Hyperspectral Image Fusion: Outcome of the 2022 WHISPERS Hyperspectral Pansharpening Challenge

Gemine Vivone, *Senior Member, IEEE*, Andrea Garzelli, *Senior Member, IEEE*, Yang Xu, *Member, IEEE*, Wenzhi Liao, *Senior Member, IEEE*, and Jocelyn Chanussot, *Fellow, IEEE*

***Abstract*—This article presents the scientific outcomes of the 2022 Hyperspectral Pansharpening Challenge organized by the 12th IEEE Workshop on Hyperspectral Image and Signal Processing: Evolution in Remote Sensing (IEEE WHISPERS 2022). The 2022 Hyperspectral Pansharpening Challenge aims at fusing a panchromatic image with hyperspectral data to get a high spatial resolution hyperspectral cube with the same spatial resolution of the panchromatic image while preserving the spectral information of hyperspectral data. Four datasets acquired by the PRISMA mission owned and managed by the Italian Space Agency have been prepared for participants. They are made available for the benefit of the scientific community. Each dataset contains a panchromatic image and a hyperspectral cube with different spatial resolutions. More than 100 registrations have been received for the event. Four teams submitted their outcomes. Since no team actually outperformed the baseline provided by the organizers, the challenge was declared inconclusive and no winner was recognized.**

***Index Terms*—Hyperspectral imaging, image fusion, optical imaging, PRISMA images, pansharpening, remote sensing, resolution enhancement.**

I. Introduction

IN THE design of optical remote sensing sensors, you cannot have your cake and eat it too. There are tradeoffs between the signal-to-noise ratio (SNR), spectral resolution, and spatial resolution. Therefore, optical remote sensing images are typically either provided with a high spatial resolution but with limited bands (e.g., panchromatic or Red-Green-Blue (RGB) images), or with high spectral resolution but with lower spatial resolution (e.g., multi-/hyperspectral images). To obtain a super image (with both high spectral and spatial resolution image), researchers have developed many methods, ranging from image super-resolution (combining multiple hyperspectral images to enhance their spatial resolution) to pansharpening. Pansharpening aims at fusion of a panchromatic image with a multi-/hyperspectral one to generate an image with the same spatial resolution of the panchromatic data and the spectral resolution of the multi-/hyperspectral image. Many applications have benefited from pansharpening, such as visual interpretation in Google Earth, land-cover and land-use mapping, and so forth.

HyperSpectral (HS) images are widely used for several tasks thanks to their very appealing spectral features. The other side of the coin is represented by the coarse spatial resolution, often limited to 30 m for satellite-based observations. To overcome this issue, recent missions, such as the Hyperspectral Precursor and Application Mission (PRISMA) owned and managed by the Italian Space Agency, have been designed to simultaneously acquire both an HS cube and a Panchromatic (Pan) image. Leveraging on the different spatio-spectral features, hyperspectral pansharpening relies upon the fusion of the abovementioned products with the aim of taking the best of them.

This research topic has been strongly debated in the last decade leading to an extensive review paper in 2015 [1] presenting a qualitative and quantitative comparison of different HS pansharpening algorithms, both considering methods originally developed for multispectral pansharpening [2] and techniques specifically designed for HS pansharpening. This study highlighted two important aspects that are still relevant today: 1) the tradeoff between computational cost (critical for images with hundreds of bands) and fusion performance; and 2) the effect of a residual space-varying registration error between the Pan band and the HS cube. When such misregistration occurs, classical pansharpening methods, mainly those based on component substitution or some specifically adapted multiresolution analysis methods, are still competitive thanks to their robustness to these issues [3], [4]. Excluding previous works on multisensor classification that did not adopt any HS pansharpening algorithm, the pioneering study about HS pansharpening was published in 2007 [5]. It proposed an optimized component substitution method, which was formalized in 2008 for multispectral

Manuscript received 8 August 2022; revised 29 September 2022; accepted 4 November 2022. Date of publication 10 November 2022; date of current version 7 December 2022. *(Corresponding author: Gemine Vivone.)*

Gemine Vivone is with the Institute of Methodologies for Environmental Analysis, National Research Council-IMAA, 85050 Tito, Italy (e-mail: gemine.vivone@imaa.cnr.it).

Andrea Garzelli is with the Department of Information Engineering and Mathematics, University of Siena, 53100 Siena, Italy (e-mail: andrea.garzelli@unisi.it).

Yang Xu is with the School of Computer Science and Engineering, Nanjing University of Science and Technology, Nanjing 210094, China (e-mail: xuyangth90@njust.edu.cn).

Wenzhi Liao is with the Flanders Make and Ghent University, 8500 Kortrijk, Belgium (e-mail: wenzhi.liao@flandersmake.be).

Jocelyn Chanussot is with the CNRS, Grenoble INP, GIPSA-Lab, University Grenoble Alpes, 38000 Grenoble, France, and also with the Aerospace Information Research Institute, Chinese Academy of Sciences, Beijing 100094, China (e-mail: jocelyn.chanussot@gipsa-lab.grenoble-inp.fr).

Digital Object Identifier 10.1109/JSTARS.2022.3220974

pansharpening [6], and compared it with existing pansharpening algorithms. To the best of the authors' knowledge, it was the first paper presenting experiments on real Hyperion HS images sharpened by the concurrent Advanced Land Imager (ALI) panchromatic acquisition. Novel HS pansharpening methods appeared in the following years, either based on quality index optimization [7], or spectral preservation constraints [8]. An interesting study on the pansharpening performance on HS/Pan data acquired by the same platform or by different platforms was presented in [2]. New classical methods were then proposed, based on the guided filter [9], variational approaches [10], and a component substitution technique improved by saliency analysis [11]. Recently, the number of research papers on HS pansharpening has grown dramatically, in particular related to deep-learning [12], [13], [14], [15], [16], [17], [18], [19], [20], [21], [22], [23], [24]. Among them, it is worth citing the algorithm proposed in [21] that has been tested also at the original Pan scale on a real Hyperion/ALI dataset.

Only very few works on HS pansharpening of PRISMA images have been published so far. An application-oriented work using pansharpened PRISMA data has been presented in 2021 [25]. The goal of the proposed challenge has been to boost the research on hyperspectral pansharpening pushing researchers toward addressing more challenging issues involving the use of new data. Hence, four datasets acquired by the PRISMA mission have been prepared. Each dataset contained a Pan data and an HS image. The spatial resolution of the Pan image is 5 m. Instead, the HS sensor acquires about 250 spectral bands with a spatial resolution of 30 m.

The contest has been organized in conjunction with the 12th Workshop on Hyperspectral Image and Signal Processing: Evolution in Remote Sensing (WHISPERS). IEEE WHISPERS has the aim of bringing together all the people involved in HS data processing, i.e., everything from the acquisition, the calibration to the analysis (image processing, signal processing, feature extraction, dimension reduction, unmixing and source separation, classification). The event has also been supported by the Italian Space Agency, the Geoscience and Remote Sensing Society, and the Image Analysis and Data Fusion Technical Committee. The organizers observed a good interest, with more than one hundred registrations. However, the proposed task appeared a difficult one, especially because of the unusual ratio in the spatial resolutions (6, while most traditional pansharpening problems deal with a ratio of 4) and probably also because of the novelty of the sensor and its spectral characteristics. Eventually, only four teams submitted their results for final assessment. The four teams addressed the proposed issue exploiting innovative solutions relied upon machine learning and variational optimization-based methodologies. Despite of the use of state-of-the-art methodologies, the teams did not get outstanding results if compared with some baseline methods proposed tens of years ago for multispectral pansharpening. For this reason, the committee decided to close the contest and claim it is inconclusive (no winner).

This article presents the four datasets exploited for the challenge together with the description of the data preparation procedures (coregistration, band selection, etc.). The baseline approaches used for performance assessment of the participants' outcomes have also been described. Moreover, the article focuses attention on the protocols (both at reduced resolution and full resolution) and the related quality metrics adopted to assess the performance. Afterward, the quantitative results (both at reduced resolution and full resolution) and a qualitative analysis are shown to the readers. Finally, some further (and more general) considerations about the results of the contest and the new trends rewarding the use of artificial intelligence solutions have been proposed.

The rest of this article is organized as follows. Section II is related to the presentation of the Hyperspectral Pansharpening Challenge with the related datasets, baseline methods, and protocols for performance assessment. Instead, Section III is devoted to the description of both the quantitative and qualitative outcomes. A general discussion about hyperspectral pansharpening is also presented in Section IV. Finally, Section V concludes the article.

II. IEEE WHISPERS 2022: The Hyperspectral Pansharpening Challenge

The Italian Space Agency's PRISMA (Hyperspectral Precursor of the Application Mission) satellite was launched from the European space base in Kourou (French Guiana) on March 22, 2019. In 2020, the authors of this article conceived the idea to propose an international contest for PRISMA data exploitation. The contest, to be organized in conjunction with the Workshop on Hyperspectral Image and Signal Processing: Evolution in Remote Sensing (WHISPERS), was intended to boost the research on hyperspectral pansharpening, thanks to the spatial and spectral capabilities of the HS and Pan sensors mounted on the PRISMA platform. After the pandemic emergency, the concept became reality in conjunction with the 2022 edition of IEEE WHISPERS, taking place in Rome in September 2022. Thanks to the Italian Space Agency (ASI), four datasets have been authorized for public distribution and finally prepared for the participants. The 2022 WHISPERS Hyperspectral Pansharpening Challenge was finally launched in February 2022.

A. Datasets

Four datasets are distributed for the PRISMA contest[1], namely FR1, FR2, for pansharpening at full spatial resolution (5 m for the Pan channel, $\mathbf{P}$, and 30 m for the HS image, $\mathbf{HS}$), and RR1, RR2 for pansharpening at reduced spatial resolution (30 m for the reduced resolution Pan image, $\mathbf{P}_{\downarrow}$, and 180 m for the reduced resolution HS cube, $\mathbf{HS}_{\downarrow}$).

The datasets have been prepared for the challenge participants through the following preprocessing steps.

1) Downloading level-2-D image data product from the ASI PRISMA portal for data distribution [26]. The level-2-D product refers to the geocoded at-surface (Bottom-of-Atmosphere) reflectance data [27].

[1]Data are available at https://openremotesensing.net/knowledgebase/panchromatic-and-hyperspectral-image-fusion-outcome-of-the-2022-whispers-hyperspectral-pansharpening-challenge/

TABLE I
DATASETS

Name	Spatial size (pixels)	Number of HS bands	Geographical extension
FR1	$\mathbf{P}: 2400 \times 2400$, $\mathbf{HS}: 400 \times 400$	69	12 km $\times$ 12 km
FR2	$\mathbf{P}: 2400 \times 2400$, $\mathbf{HS}: 400 \times 400$	63	12 km $\times$ 12 km
RR1	$\mathbf{P}_{\downarrow}: 900 \times 900$, $\mathbf{HS}_{\downarrow}: 150 \times 150$	59	27 km $\times$ 27 km
RR2	$\mathbf{P}_{\downarrow}: 900 \times 900$, $\mathbf{HS}_{\downarrow}: 150 \times 150$	73	27 km $\times$ 27 km

2) Reading Visible and Near-InfraRed (VNIR) and Short-Wave InfraRed (SWIR) cubes and the Pan band according to the Hierarchical Data Format (HDF5) standard. Specific information on the PRISMA HDF5 format are available in the PRISMA products specification document [28]. The document also indicates different tools for data reading both for commercial remote sensing software packages and Python usage.
3) Removing atmospheric water absorption bands, low signal-to-noise ratio (SNR) bands, and bands affected by severe striping, which is due to a temporary unbalanced response of a VNIR or SWIR detector.
4) Assembling the selected VNIR and SWIR bands into a single image cube spanning the VNIR and SWIR wavelength range. The final number of bands varies among the four datasets, as reported in Table I.
5) Correcting any residual space-varying misalignment between the HS bands and the Pan band through local correlation computation and nonrigid transformation. This operation has been performed by interpolating the HS bands at the 5-m panchromatic scale through bicubic interpolation and by using the Sentinel-2 temporally closest acquisition as reference. Sentinel-2 band 4 at 665 nm is bicubically interpolated first at 5 m and then used as a common reference for displacement estimation of the 660 nm PRISMA band and the Pan band. It should be noted that the estimated displacement between the 660-nm band of PRISMA and the Sentinel-2 B4 band is finally used for all VNIR and SWIR bands of PRISMA, which are perfectly coregistered in the original ASI product.

The images $\mathbf{P}$ and $\mathbf{HS}$ of the full resolution datasets FR1 and FR2 have been obtained by extracting a 12 km $\times$ 12 km portion (2400×2400 pixels for $\mathbf{P}$ and $400 \times 400 \times N$ pixels for $\mathbf{HS}$) from the original 30 km $\times$ 30 km PRISMA acquisition, after accurate coregistration.

The 900×900 $\mathbf{P}_{\downarrow}$ image and the coregistered $150 \times 150 \times N$ $\mathbf{HS}_{\downarrow}$ denote the 30 m resolution Pan image and the N-band 180 m resolution HS image on a geographical area of 27 km $\times$ 27 km.

$\mathbf{P}_{\downarrow}$ has been obtained from the original $\mathbf{P}$ by using an ideal antialiasing low-pass filter, while $\mathbf{HS}_{\downarrow}$ has been produced from the original HS by applying spatial filters matching the sensor's Modulation Transfer Functions (MTFs) of the VNIR and SWIR bands.

For easy portability, images are in ENVI format, that is, a flat-binary raster file in 16-b unsigned integer data format and Band Sequential (BSQ) interleave type, with an accompanying ASCII header file. Each HS image contains N bands selected from the original VNIR-SWIR PRISMA bands. The ASCII header also contains the values of the central wavelengths of the HS bands.

Table I reports the main characteristics of the four datasets in terms of spatial size, number of bands, and geographical extension.

Fig. 1 shows the Pan bands and true-color composites from the HS image of the four datasets.

FR1 denotes the PRISMA acquisition over the city of Bologna, Italy, and its surroundings, on November 7, 2020. The FR2 dataset was acquired over the Florence area (Italy) on June 27, 2020. For the abovementioned cases, the spatial resolutions of the Pan and HS bands are those of the original acquisitions, i.e., 5 and 30 m, respectively.

RR1 denotes the acquisition over the city of Barcelona (Spain) on January 24, 2020, while RR2 corresponds to the PRISMA acquisition on August 13, 2020, over the suburbs of Milan, Italy. The latter two datasets are composed of spatially degraded images, whose characteristics are recalled in Table I.

The four datasets, together with a Matlab toolbox for testing and evaluating the baseline methods, are publicly available at [29].

B. Baseline Methods

Five methods are exploited as baseline solutions in this challenge. The code of the baseline solutions is made available to the scientific community.[2] They have been borrowed from the pansharpening literature [2] and successively used for addressing the hyperspectral pansharpening task [1].

The first two methods belong to the component substitution class [30], [31]. More specifically, the Gram-Schmidt (GS) approach [32] is considered. This is a quite dated solution relied upon the substitution of the first component of the HS cube after the GS transformation. The high resolution Pan image (with adjusted statistics) is substituted to get the resolution enhancement. The fused image is obtained by the inverse GS transformation on the new set of transformed components. The second technique (an enhanced version of the GS) is based on the same transformation (i.e., the GS one) but improving it using a liner model for the intensity (first) component. The GS Adaptive (GSA) [33] synthesizes an intensity component using a linear model, properly estimating its weights through the relationship between the HS image and a low-pass filtered and decimated

[2]The code is available at https://openremotesensing.net/knowledgebase/panchromatic-and-hyperspectral-image-fusion-outcome-of-the-2022-whispers-hyperspectral-pansharpening-challenge/

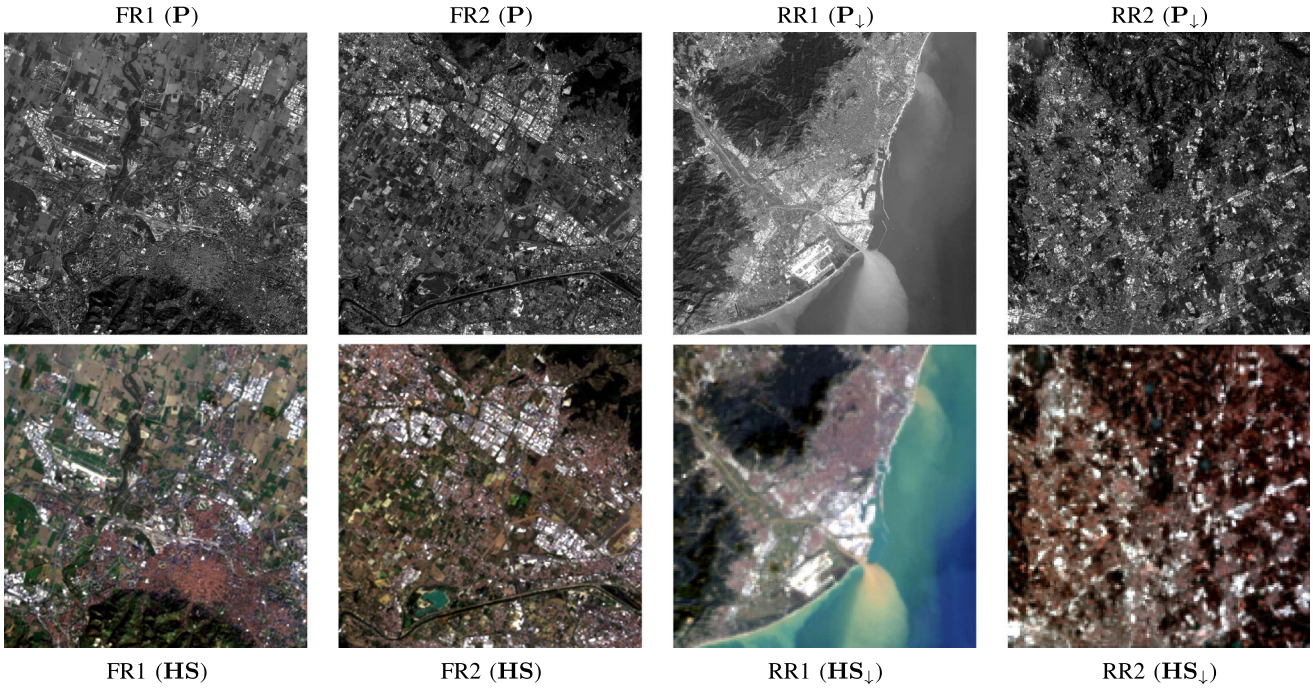

Fig. 1. Challenge datasets: 5 m Pan and 30 m HS bands have been provided for FR1 and FR2; 30 m Pan and 180 m HS have been provided for RR1 and RR2. True-color composites are shown for HS data.

version of the Pan data. This component represents the first basis defining the transformed domain and it is used to project the HS cube. Again, the fused image is obtained by substituting the component related to the linear model with the Pan image and inverting the transformation.

The other three baseline methods are representative of the multiresolution analysis class [30], [31]. The third method is the classical Additive Wavelet Luminance Proportional (AWLP) [31], [34]. The wavelet planes of the Pan image are added to the luminance component of the HS image. The adopted injection rule is based on the idea to have proportionality between each HS band and the injected details, thus preserving the spectral signature. The fourth technique is the MTF–Generalized Laplacian Pyramid (MTF-GLP) [31], [35]. It exploits GLPs to extract details from the Pan image. The Gaussian filters are designed to match the HS sensor's MTFs [35]. A linear regression model [31] is used to address the details injection problem. Finally, the last method is the Morphological Filters (MF) [36]. It relies upon a nonlinear decomposition scheme using half gradient MFs. A multiplicative injection model is exploited to complete the fusion procedure [37].

It is worth to be remarked that machine learning-based approaches are not adopted as baseline methods. Indeed, their use with data having different spatio-spectral features (e.g., a different number of spectral bands) often requires changes in the original network architectures and their retraining to properly address the problem at hand. Thus, the application of these approaches to the fusion of PRISMA data is not straightforward.

C. Protocols

The assessment of image fusion products is a hard problem with a nontrivial solution. Since 30 years ago, researchers have studied the topic proposing ways to address it considering its ill-posed nature. Indeed, the assessment at the working (full) resolution leads to the absence of a reference (ground-truth) image that is the image that the HS sensor would observe with the highest spatial resolution (i.e., the one of the Pan sensor). This is the so-called synthesis property of Wald's protocol [38], which is hard to be measured without a reference. Thus, several indexes, inspired by the quality without reference (QNR) protocol [39], have been proposed in the literature. These metrics leverage on working at full resolution, but paying it with often inaccurate evaluations because of the absence of a reference (ground-truth) image. Thus, to complete the assessment, an evaluation at reduced resolution is crucial (with the aim of implementing Wald's protocol) to generate a reference image (i.e., the original HS cube). The assumption under this kind of assessment is an invariance among scales of the performance of the pansharpening approach under evaluation, i.e., a method showing some performance at reduced resolution should have the same behavior at finer resolution. Obviously, this hypothesis is not always valid and the process of reducing input data resolutions can represent a degree of freedom, often unacceptable for a validation procedure (even though step forwards have been done imposing the design of filters taking into account the spatial models of the acquisition sensors [35]). Thus, considering the pros and cons of both the procedures, this challenge relies upon a protocol accounting for both reduced and full resolution assessments to have a complete evaluation of the submitted outcomes. Finally, a visual inspection of fused products have also been performed to highlight local patterns and distortions, in particular for full resolution outcomes.

Reduced resolution assessment measures the similarity of the fused product to an ideal reference, i.e., the original HS

image. That is possible by degrading the resolutions of both the original HS and Pan images, and by performing fusion from those degraded data. Clearly, the choice of the filter is crucial in this validation protocol. The filter is defined for ensuring the consistency property [38] of the pansharpening process. Thus, it is straightforward that the resolution reduction of the HS image should be done by exploiting spatial filters matching the HS sensor's MTFs [30].[3] In addition, the filter used to degrade the Pan image should be designed to preserve the details that would have been seen if the image were acquired at reduced resolution. Accordingly, a common choice is the use of an almost ideal filter [30]. The more similar is the obtained pansharpened image to the original HS image, the higher is the measured quality. Such a similarity degree can be easily computed through score indexes that compare two multiband images. In this challenge, we use the following set of well-established metrics [30], [31].

1) Spectral Angle Mapper (SAM) [30], [31], [40]. Given two spectral vectors, $\mathbf{v}$ and $\hat{\mathbf{v}}$, both having N components, in which $\mathbf{v} = [v_1, v_2, \ldots, v_N]$ is the reference spectral pixel vector and $\hat{\mathbf{v}} = [\hat{v}_1, \hat{v}_2, \ldots, \hat{v}_N]$ is the test spectral pixel vector, the SAM denotes the absolute value of the spectral angle between the two vectors

$$\text{SAM}(\mathbf{v}, \hat{\mathbf{v}}) = \cos^{-1} \frac{< \mathbf{v}, \hat{\mathbf{v}} >}{||\mathbf{v}||_2 \cdot ||\hat{\mathbf{v}}||_2} \tag{1}$$

where $< \cdot, \cdot >$ indicates the dot product, $\cos^{-1}$ denotes the arccosine function, and $|| \cdot ||_2$ is the ℓ_2 norm. The SAM is usually expressed in degrees. The lower the value, the better the quality. The SAM is equal to zero if and only if the test vector is spectrally identical to the reference vector, i.e., the two vectors are parallel and may differ only by their moduli. A global spectral dissimilarity, or distortion, index is obtained by averaging the index over the whole scene.

2) ERGAS [30], [31], [41]. The index, whose French acronym stands for relative dimensionless global error in synthesis, is a normalized dissimilarity index that offers a global indication of the distortion toward the reference of a test multiband image

$$\text{ERGAS} = 100 \frac{d_h}{d_l} \sqrt{\frac{1}{N} \sum\nolimits_{n=1}^{N} \left(\frac{\text{RMSE}(n)}{\mu(n)} \right)^2} \tag{2}$$

where d_h/d_l is the ratio between pixel sizes of Pan and HS; $\mu(n)$ is the mean (average) of the nth band of the reference; $RMSE(n)$ is the root mean square error (RMSE) calculated between the fused and the reference images for the nth spectral band; and N is the number of bands. Low values of the ERGAS indicate high similarity between fused and reference HS data. The ideal value is zero.

3) $Q2^n$ [30], [31], [42]. It is the multiband extension of the Universal Image Quality Index (UIQI). Each pixel of an image with N spectral bands is accommodated into a HyperComplex (HC) number with one real part and $N-1$ imaginary parts. Let $\mathbf{z} = \mathbf{z}(m,n)$ and $\hat{\mathbf{z}} = \hat{\mathbf{z}}(m,n)$ denote the HC representation of the reference and test spectral vectors at pixel (m,n). Analogously to UIQI, namely, $Q2^0 = Q$, $Q2^n$ can be written as the product of three terms

$$Q2^n = \frac{|\sigma_{\mathbf{z},\hat{\mathbf{z}}}|}{\sigma_{\mathbf{z}}\sigma_{\hat{\mathbf{z}}}} \cdot \frac{2\sigma_{\mathbf{z}}\sigma_{\hat{\mathbf{z}}}}{\sigma_{\mathbf{z}}^2 + \sigma_{\hat{\mathbf{z}}}^2} \cdot \frac{2|\bar{\mathbf{z}}||\bar{\hat{\mathbf{z}}}|}{|\bar{\mathbf{z}}|^2 + |\bar{\hat{\mathbf{z}}}|^2} \tag{3}$$

where $\sigma_{\cdot,\cdot}$, $\sigma_{\cdot}$, and $\bar{\cdot}$ denote the covariance, the standard deviation, and the mean operators, respectively, and $|\cdot|$ represents the modulus of a vector. The first term is the modulus of the HC Correlation Coefficient (HCCC) between $\mathbf{z}$ and $\hat{\mathbf{z}}$. The second and the third terms measure contrast changes and mean bias, respectively, on all the bands simultaneously. Statistics are calculated on $N \times N$ blocks, typically, 32×32, and $Q2^n$ is averaged over the blocks of the whole image to yield the global score index. $Q2^n$ takes values in $[0, 1]$ and is equal to 1 if and only if $\mathbf{z} = \hat{\mathbf{z}}$ for all the pixels.

Full resolution assessment infers the quality of the pansharpened image at the Pan resolution without resorting to a single reference image, which is not available. Consequently, the problem of assessing the quality of pansharpened products at full resolution is intrinsically ill-posed. To solve this issue, new distortion measurements have been introduced, such that they do not depend on the unavailable high resolution HS cube. The Q^* index [43] is defined as

$$Q^* = \left(1 - D_\lambda^k\right)^\alpha \cdot \left(1 - D_S^*\right)^\beta \tag{4}$$

which is composed by the product of D_λ^k and D_S^*, quantifying the spectral and the spatial distortions, respectively, exploiting the weights α and β (both experimentally set to 1). The higher the Q^* index, the better the quality of the fused product. The maximum theoretical value of this index is 1 when both D_λ^k and D_S^* are equal to zero.

The spectral distortion index is calculated as follows [30], [43]:

$$D_\lambda^k = 1 - Q(\widehat{\mathbf{HS}_\downarrow}, \widetilde{\mathbf{HS}}) \tag{5}$$

where $\widehat{\mathbf{HS}_\downarrow}$ is the MTF-filtered pansharpened HS image considering a resolution ratio equal to R; $\widetilde{\mathbf{HS}}$ is the original HS image interpolated to the Pan scale (R times lower than the HS scale); and Q is the UIQI averaged along the HS spectral bands.[4]

Instead, the spatial consistency, $1 - D_S^*$, proposed in [44], is defined by the multivariate linear regression modeling the relationship between the original high resolution Pan and the pansharpened HS bands. The figure of merit of the matching between the abovementioned images is given by the coefficient of determination that is used to measure the spatial consistency [44]. The choice of this combination of metrics for measuring spatial and spectral qualities has also been corroborated

[3]The assumption is that the HS sensor's MTFs follow a Gaussian shape and the standard deviation is set thanks to the information given by data providers about the gains at Nyquist frequency that are all equal to 0.3 in this case.

[4]It is worth to be remarked that the original implementation of D_λ^k is based on the use of the $Q2^n$ index instead of the average of Q metrics calculated for each spectral band. This modification has been provided for computational reasons considering the high number of HS bands leading to a very slow evaluation of the $Q2^n$ index. Anyway, comparable performance can be obtained by this modification with a relevant advantage from a computational burden point of view.

TABLE II
RESULTS ON THE RR1 DATASET INCLUDING $Q2^n$, SAM, AND ERGAS

	$Q2^n$	SAM	ERGAS
EXP	0.5740	**3.3203**	3.6816
GS [32]	0.5080	14.1040	7.9535
GSA [33]	**0.6912**	3.3297	**2.8750**
AWLP [31]	0.6166	4.8929	4.1890
MTF-GLP [35]	0.6207	3.6398	3.9223
MF [36]	0.6189	5.5063	7.2229
Team 1	0.1286	10.5527	41.0279
Team 2	0.5263	3.7735	5.1628
Team 3	0.6849	4.1293	3.3394
Team 4	0.6402	5.0922	3.9272

Best results are in boldface. Best results among the four teams are underlined.

TABLE III
RESULTS ON THE RR2 DATASET INCLUDING $Q2^n$, SAM, AND ERGAS

	$Q2^n$	SAM	ERGAS
EXP	0.5717	6.1252	7.0178
GS [32]	0.7221	5.5997	5.9123
GSA [33]	**0.8251**	**4.8277**	**4.4092**
AWLP [31]	0.6935	7.6157	5.9395
MTF-GLP [35]	0.7963	5.3705	4.7784
MF [36]	0.8057	5.2975	4.7005
Team 1	0.1280	14.0155	81.3597
Team 2	0.7595	5.3577	5.1664
Team 3	0.8137	5.2395	5.2888
Team 4	0.7341	6.7361	5.0231

Best results are in boldface. Best results among the four teams are underlined.

for classical pansharpening in [43]. The code for assessing the performance both at reduced resolution and at full resolution is made available to the scientific community.[5]

III. OUTCOMES OF THE IEEE WHISPERS 2022 HYPERSPECTRAL PANSHARPENING CHALLENGE

This section is devoted to the presentation of the results of the IEEE WHISPERS 2022 challenge on hyperspectral pansharpening. The quantitative assessment will be presented first under the protocol defined in Section II-C. Four datasets (two at reduced and two at full resolutions) have been shared with the participants. The quality metrics have been calculated for both the baseline methods and the outcomes provided by the teams joining the challenge. Moreover, a qualitative assessment of the delivered products has been proposed in this section. This is done to support the assessment, in particular at full resolution. Finally, in Section III-C, a general discussion on the obtained outcomes is reported.

A. Quantitative Assessment

Four datasets have been considered for this challenge. All the images are captured by sensors onboard of the PRISMA mission. Two datasets refer to the reduced resolution assessment (named RR1 and RR2), instead, the other two are at full resolution data (called FR1 and FR2). Baseline approaches, as presented in Section II-B, have been run on the four datasets. The performance at reduced resolution and at full resolution for both baseline approaches and the outcomes provided by the participants is measured according to the protocol described in Section II-C.

The results at reduced resolution are reported in Tables II and III for the RR1 and RR2 datasets, respectively. Having a look at the overall $Q2^n$ index, we can remark very similar results between the two datasets. Indeed, the best approach is always the GSA followed by Team 3's one. Instead, the worst method is always the one provided by Team 1. The ERGAS index, even though measuring a different quantity (just a radiometric distortion in ℓ_2), is generally in agreement with the findings of the $Q2^n$. Again, the best approach is represented by the GSA and the worst results are related to Team 1.[6] Focusing on teams' outcomes, again, Team 1 is the worse followed by Team 2. Instead, more comparable performance can be obtained by Teams 3 and 4 representing the best results among the teams' ones. The last consideration is about the spectral distortion measured by the SAM index. Generally speaking, results seem to be much more dependent on the scenario and an overall evaluation turns out to be more complicated. Just focusing on the teams, again, Team 1 is the worse showing a relevant spectral distortion of the results. Among the other methods, the highest results of the SAM index are obtained by Team 4. Instead, the products of Team 2 and Team 3 seem to be more spectral consistent.

TABLE IV
RESULTS ON THE FR1 DATASET INCLUDING D_λ^k, D_S^*, AND Q^*

	D_λ^k	D_S^*	Q^*
EXP	**0.0174**	0.2889	0.6987
GS [32]	0.2648	0.0113	0.7269
GSA [33]	0.0512	0.0121	0.9373
AWLP [31]	0.0274	0.0490	0.9249
MTF-GLP [35]	0.0396	0.0341	0.9277
MF [36]	0.0939	0.0663	0.8460
Team 1	0.6331	**0.0008**	0.3666
Team 2	0.0831	0.0134	0.9046
Team 3	0.0837	0.0360	0.8833
Team 4	0.0338	0.0269	**0.9402**

Best results are in boldface. Best results among the four teams are underlined.

The results at full resolution are instead reported in Tables IV and V for the FR1 and FR2 datasets, respectively. As for the

[5]The code is available at https://openremotesensing.net/knowledgebase/panchromatic-and-hyperspectral-image-fusion-outcome-of-the-2022-whispers-hyperspectral-pansharpening-challenge/

[6]In this case, the gap in performance of Team 1's results with the other outcomes is even larger due to the unbounded nature of this index.

TABLE V
RESULTS ON THE FR2 DATASET INCLUDING D_λ^k, D_S^*, AND Q^*

	D_λ^k	D_S^*	Q^*
EXP	**0.0159**	0.2415	0.7464
GS [32]	0.2073	0.0344	0.7654
GSA [33]	0.0555	0.0033	0.9414
AWLP [31]	0.0257	0.0367	0.9385
MTF-GLP [35]	0.0331	0.0254	0.9423
MF [36]	0.1044	0.0447	0.8556
Team 1	0.4900	**0.0006**	0.5097
Team 2	0.1055	0.0108	0.8849
Team 3	0.0876	0.0131	0.9004
Team 4	0.0336	0.0168	**0.9501**

Best results are in boldface. Best results among the four teams are underlined.

TABLE VI
OVERALL ACCURACY (OA) OBTAINED BY AVERAGING THE OVERALL QUALITY INDEXES AT FULL AND AT REDUCED RESOLUTIONS, I.E., Q^* AND $Q2^n$, RESPECTIVELY

	OA
EXP	0.6477
GS [32]	0.6806
GSA [33]	**0.8488**
AWLP [31]	0.7934
MTF-GLP [35]	0.8218
MF [36]	0.7816
Team 1	0.2832
Team 2	0.7688
Team 3	0.8206
Team 4	0.8162

Best results are in boldface. Best results among the four teams are underlined.

assessment at reduced resolution, focusing on the overall quality metric, Q^*, we got quite similar results on FR1 and FR2. Indeed, the best approach is always represented by the one of Team 4 followed by two baseline techniques, i.e., GSA and MTF-GLP. Comparable performance is reported for the techniques provided by Teams 2 and 3. Again, Team 1 got the worst overall performance, but showing the best spatial consistency, thanks to the estimation of linear-based spatial and spectral responses following the approach proposed in [45]. However, the best performance on this index is not enough to get the overall good performance because of the relevant spectral distortion. From a spectral distortion point of view, the best approach is the simple upsampling with bicubic interpolation (named EXP) thanks to the fact that no injection of spatial details is performed, thus, avoiding the introduction of spectral distortion in this phase (as in the case of the other compared methods).

The overall results, exploited to define the ranking in Table VII, are obtained taking into account the overall quality indexes both at reduced resolution and at full resolution. More specifically, the $Q2^n$ is taken at reduced resolution representing a good candidate to give a big picture considering both radiometric and spectral distortions in the fused products. Instead, at full resolution, the unique metric representing an overall accuracy is the Q^* index obtained by combining the spatial (D_S^*) and spectral (D_λ^k) distortions. Since we combined two Q-like metrics (i.e., $Q2^n$ and Q^*), the final overall accuracy is simply obtained by averaging these metrics calculated for RR1 and RR2 ($Q2^n$) and for FR1 and FR2 (Q^*). The results are reported in Table VI. The best results are reached by the GSA method followed by the MTF-GLP approach. Teams 3 and 4 obtained high performance getting the third and fourth positions, respectively. Team 3 is the best among the participants' approaches showing a good balance in performance and robustness varying the assessment procedure and scenario under test. Instead, Team 4 has the best performance at full resolution paid by a lower accuracy at reduced resolution (in particular on the RR1 test case). Medium performance is instead shown by the outcomes provided by Team 2. Finally, the worst performance (worse than the simple upsampling approach, EXP) is reached by Team 1.

B. Qualitative Assessment

The results on the four datasets of the challenge, namely FR1 and FR2 for the full resolution assessment and RR1 and RR2 for the reduced resolution assessment, are displayed and compared in this section for qualitative, visual evaluation.

Fig. 2 shows a 512×512 fragment of the FR1 scene. A true-color representation, a color composition in the SWIR and NIR wavelengths, both at the original 30-m resolution, and the 5-m Pan band are reported. The true-color pansharpening result of a baseline method, namely the GSA [33], is also shown in Fig. 2. This color composite is displayed with the same visualization parameters of the true-color upsampled image to visually evaluate the spectral quality of the fused image. Since a reference image is not available for full resolution assessment, the GSA result, which achieved the best score indexes among the tested algorithms (Tables VI–VII), is reported in Fig. 2 for useful comparison with the challenge results illustrated in Fig. 3.

Fig. 3 shows the results obtained by the four teams on the FR1 dataset. Each image is displayed with linear stretching between 1% and 99% of the histogram range for each band. The same visualization parameters used for the true-color composites in Fig. 2 cannot be applied to the fusion results produced by the four teams, due to mean bias (significant for Team 1) between original and pansharpened bands. As an example, the histograms of the 478-nm band before and after Team 1's pansharpening are shown in Fig. 4.

In this way, Fig. 3 allows for a fair comparison of the results from the different teams at their best visualization conditions.

Team 1's result appears sharp but presenting spectral distortions in the vegetated area, particularly evident in the true-color composition. Comparisons with Fig. 2 confirm the numerical results of Table IV. Superior spectral quality is shown by Team 4, both from the true-color and the false-color compositions.

TABLE VII
FINAL RANKING

Ranking	1	2	3	4	5	6	7	8	9	10
Method	GSA	MTF-GLP	Team 3	Team 4	AWLP	MF	Team 2	GS	EXP	Team 1

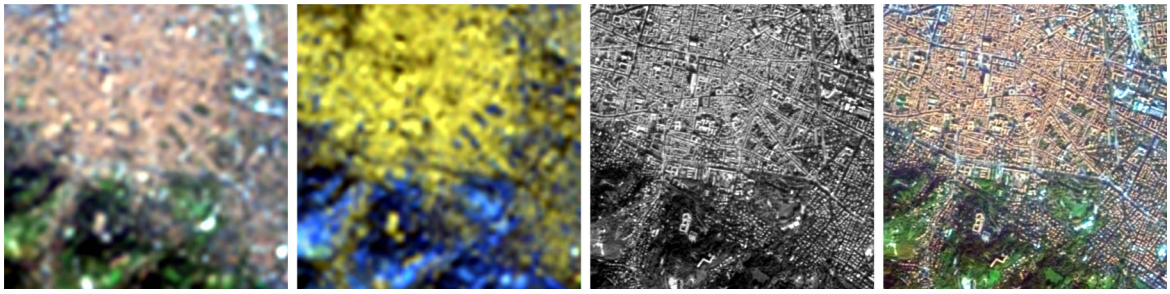

Fig. 2. 512×512 portions of the FR1 dataset. From left to right: Color composites of the original HS image resampled at Pan scale, true-color (641, 563, 478) nm and false-color (1586, 1229, 770) nm; Pan image; true-color GSA-pansharpened image [33].

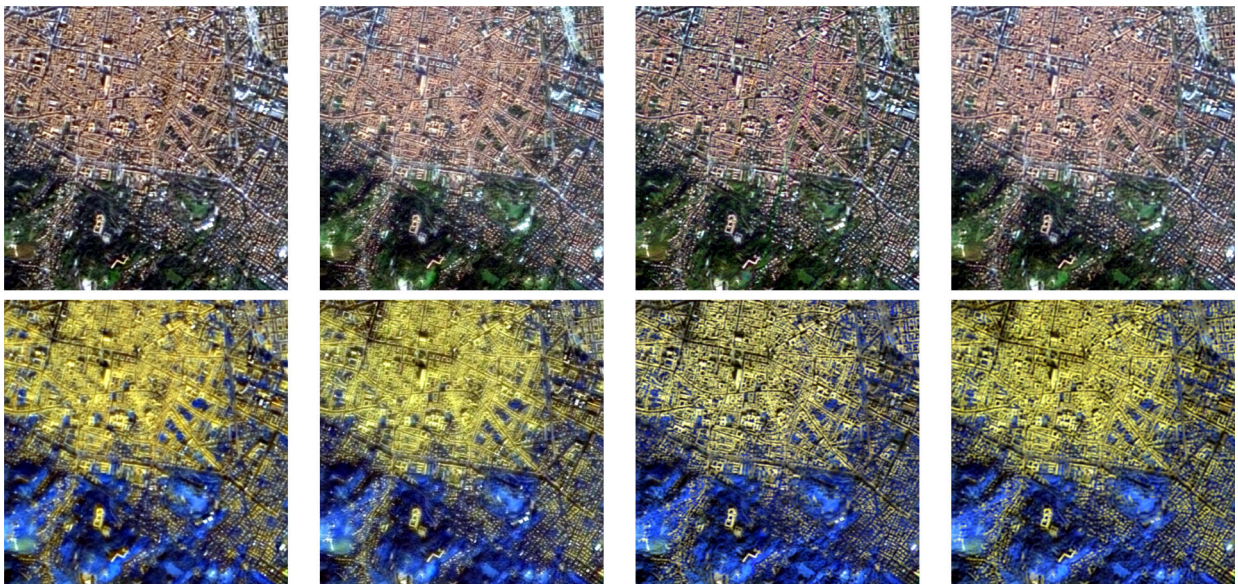

Fig. 3. Pansharpening results on a 512 × 512 portion of the FR1 dataset with color composites displayed in Fig. 2. Linear stretching between 1% and 99% of the histogram range for each band is used for visualization.

A common problem of the products by Teams 1, 2, and 3, but not Team 4, is the injection of residual striping artifacts into the displayed bands. This problem is evident in the true-color representation.

The results for the FR2 dataset are reported in Figs. 5–6. The spectral distortion introduced by Team 1's pansharpening algorithm can be appreciated on the rooftops of the residential area in the lower part of the image, both for true-color and false-color representations. On the other hand, the spatial details injection of the Team 1 product is efficient. For comparison, see the bottom images of Teams 2–4 that appear less sharpened. Similarly to the FR1 dataset, also the FR2 visual assessment reveals that Team 4 better preserves the spectral information.

The results for the RR1 dataset are shown in Figs. 8–9. Here, a direct visual comparison of the challenge results from the four teams and the original (reference) image in Fig. 8 is possible. Spectral distortion is severe for the pansharpened images by Teams 1, 3, and 4. As an example, the spectral information of the river appears highly distorted in products provided by Teams 1 and 4, particularly in the false-color representation at (2053,1555,855) nm wavelengths (bottom of Fig. 9). The Team 2 outcome shows insufficient spatial details injection, which is more evident in the true-color representation. Fig. 7 instead shows the spectral signatures of the ground-truth and the ones obtained by the compared approaches for three selected points representing three different kinds of landscape (i.e.,

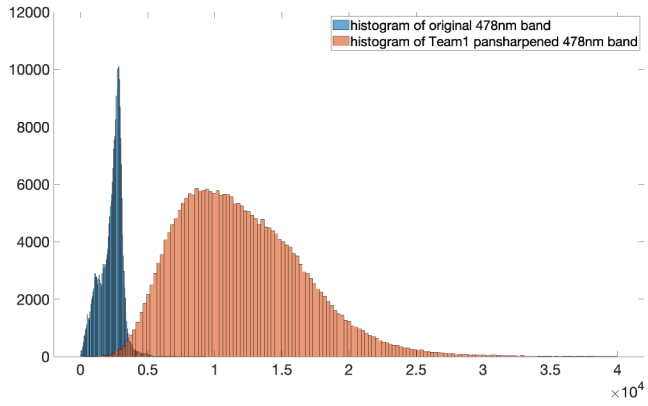

Fig. 4. Histograms of original and Team 1's pansharpened band at 478 nm of the FR1 dataset.

urban, vegetated, and mixed). The closer the spectral signatures with respect to the ground-truth, the better the results. It is easy to be remarked that the best results are obtained by the EXP method followed by the GSA in agreement with the SAM values in Table II.

Figs. 10 and 11, concerning the RR2 dataset, confirm the visual analysis on the RR1 dataset. Team 1's result is severely spectrally distorted, while Team 2's pansharpened image suffers from underenhancement of the spatial details extracted from the Pan image. Team 3 and 4's products show significant spectral distortions, more evident in the true-color image for Team 3 and in the false-color (one NIR and two SWIR wavelengths) for Team 4.

C. Discussion on Challenge Results

Spectral information is of paramount importance in hyperspectral imaging. A discussion on the challenge results presented by the four teams should start from specific considerations about the preservation of the spectral information of the original HS image after the spatial enhancement through hyperspectral pansharpening. This kind of assessment is straightforward on the two datasets at reduced resolution, since a reference HS image, the original image at 30 m resolution, is available. It is evident from an objective assessment in Tables II–III and visual analysis in Figs. 8–9 for the RR1 dataset, and Figs. 10–11 for the RR2 dataset, that the Team 1 algorithm introduces significant spectral distortions, and Teams 2, 3, and 4 are almost equivalent, since Team 4 outperforms the others on the RR1 dataset, but not on the RR2 dataset (see, e.g., the poor spectral fidelity of the false-color composite in Fig. 11). In summary, the results by all the teams are spectrally insufficient, since the lowest value of the SAM index for the RR1 and RR2 datasets (and the most spectrally consistent color compositions in the visible, NIR, and SWIR wavelengths) are provided by the baseline GSA method. This conclusion is confirmed by the results at full resolution, where the Team 4 results show an acceptable spectral behavior.

Similarly to spectral quality, spatial enhancement can be easily assessed on the reduced resolution datasets, RR1 and RR2, through direct comparison with the original 30-m image and computation of multiband quality indexes. Team 3 provides the best results in term of injection of spatial details. This is proved by the score indexes in Tables II–III and confirmed by comparing the reference images in Figs. 8 and 10 and the sharpened images in Figs. 9 and 11, respectively. More significant is the evaluation of the spatial quality at full resolution, when a 5-m HS image is synthesized. Close-ups in Figs. 3 and 6 show sharp images from Team 1, comparable results from Teams 3 and 4, and insufficient details injection provided by Team 2's method. This consideration is in accordance with the computed score indexes in Tables IV and V.

As pointed out in Section III-A, all the teams presented pansharpened HS images with lower overall quality with respect to the baseline GSA method.

IV. Hyperspectral Pansharpening: Where are We Now? A Discussion on the Challenge

This contest puts a spotlight on the hyperspectral pansharpening problem pushing researchers in finding solutions to a well-known problem in the image fusion literature, but involving new data. Indeed, PRISMA images are not widely used in the related scientific community and this represents a further challenge, i.e., the development of the best hyperspectral pansharpening approach for a new set of data. This implies that there is no prior knowledge about the particular problem at hand together with the absence of pretrained models for machine learning-based approaches.

In this context, the four teams addressed the issue proposing innovative solutions relied upon machine learning and variational optimization-based methodologies, sometimes borrowed by the related multispectral and hyperspectral image fusion literature. Anyway, despite the use of state-of-the-art methodologies, such as deep networks (which already demonstrated high performance for closely related tasks), the teams did not get outstanding results if we compare them with some baseline methods that were proposed tens of years ago in the multispectral pansharpening literature (see, e.g., the GSA and the MTF-GLP). For this reason, the committee decided to close the contest and claim it is inconclusive (no winner).

Generally speaking, the organizers observed a good interest (with more than 100 registrations) for this challenge, but just four submissions. One of the reasons could be found in the fact that some researchers are more prone to tune fusion approaches with trial and error procedures and this contest does not provide this opportunity because of the absence of ground-truth samples. The lack of ground-truth samples was even more critical in this challenge because of the specific nature of the data (new sensor with specific spectral coverage and specific ratio for the spatial resolutions), hence preventing deep networks pretrained with data provided by other satellites from providing useful estimates. In particular, machine learning approaches usually require a tuning phase for hyperparameters that is often addressed treating the networks as black-boxes and driving the tuning process through improving a quality metric on ground-truth samples. Unfortunately, an evaluation server (which continuously assesses the performance on test cases) was not set up for this

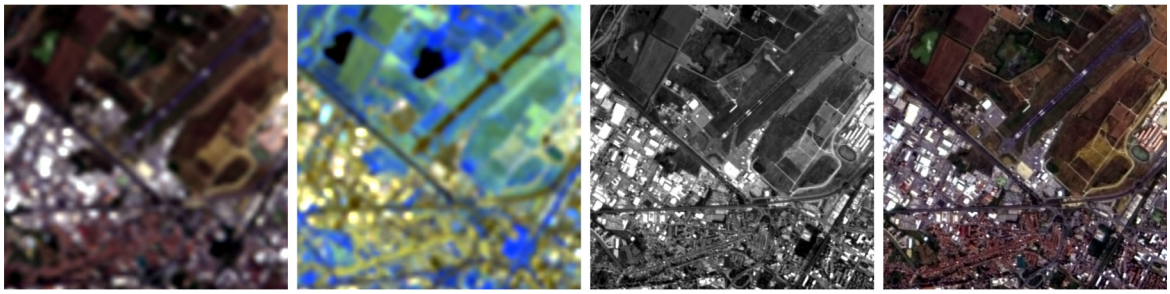

Fig. 5. 512×512 portions of the FR2 dataset. From left to right: Color composites of the original HS image resampled at panchromatic scale, true-color (641, 563, 456) nm and false-color (2053, 1284, 802) nm; Pan image; true-color GSA-pansharpened image [33].

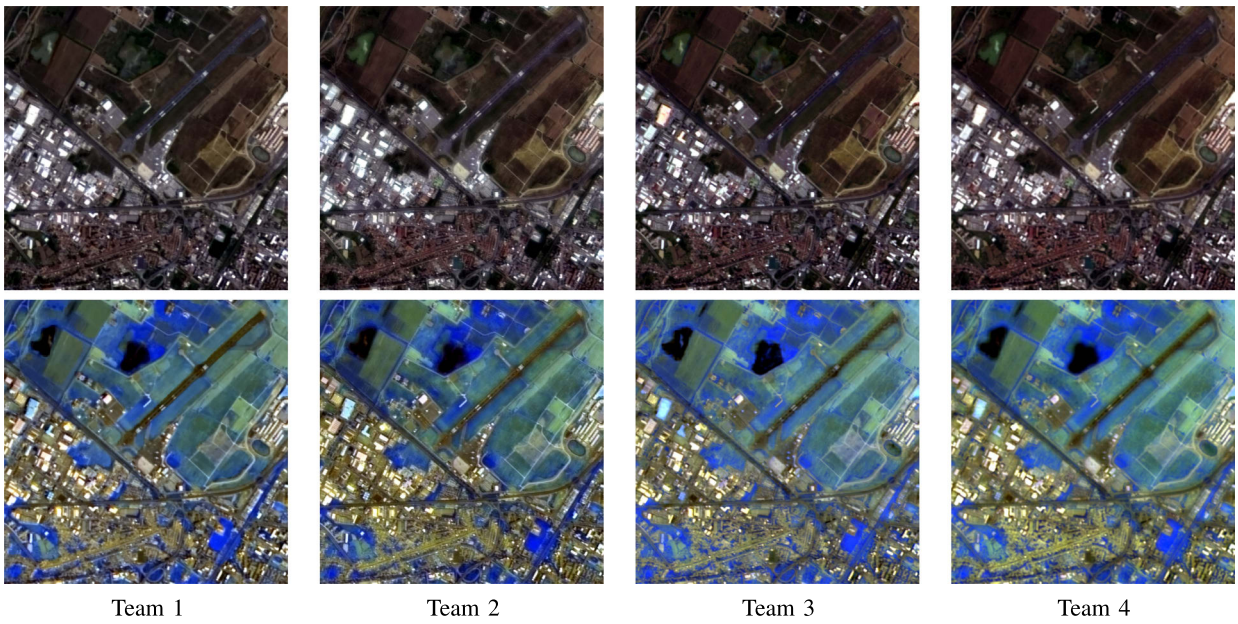

Fig. 6. Pansharpening results on a 512×512 portion of the FR2 dataset with color composites displayed in Fig. 5. Linear stretching between 1% and 99% of the histogram range for each band is used for visualization.

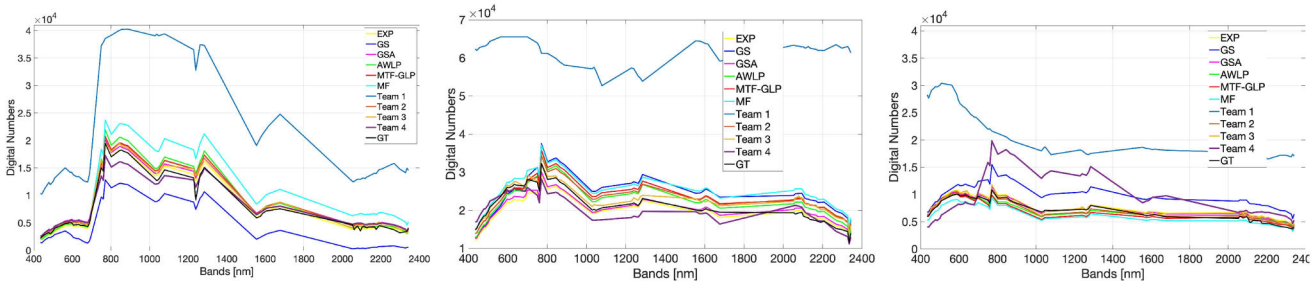

Fig. 7. Spectral signatures obtained on (a) vegetation, (b) urban, and (c) mixed pixel samples from the RR1 dataset.

challenge, as done for other well-known contests as the Data Fusion Contest organized by the IEEE GRSS Image Analysis and Data Fusion Technical Committee. In the opinion of the organizers, the absence of ground-truth samples (related to the testing scenarios) and an evaluation server (following the line drawn by other contests) limited the possibility of fine-tuning for the proposed approaches, thus, reducing the performance.

This last point opens the door to some general considerations about the use of machine learning-based approaches to solve image sharpening problems. Indeed, it is not seldom to see

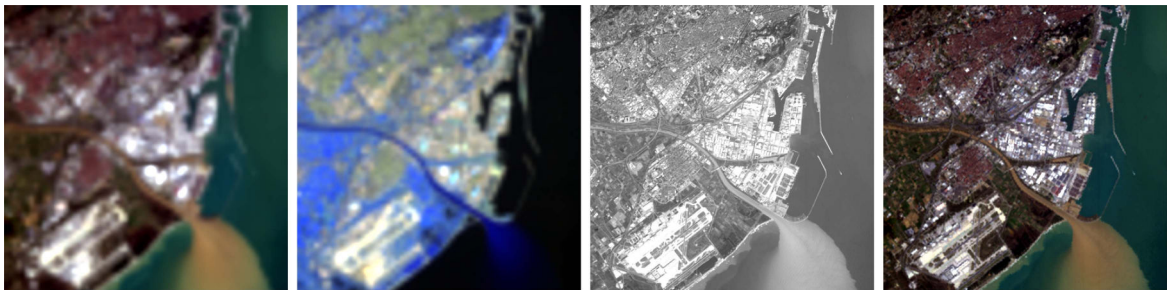

Fig. 8. 400×400 portions of the RR1 dataset. From left to right: Color composites of the HS image degraded at 180 m and resampled at 30 m, true-color (641, 563, 478) nm and false-color (2053, 1555, 855) nm; Pan image degraded at 30 m; true-color original at 30 m (reference, not distributed).

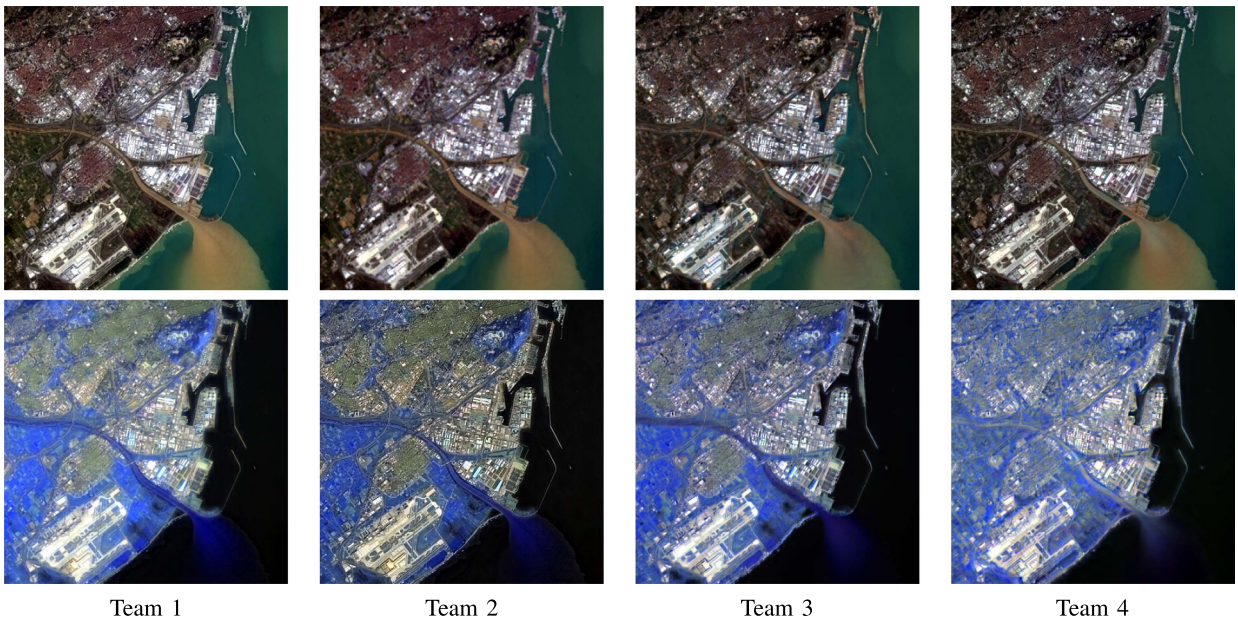

Fig. 9. Pansharpening results on a 400×400 portion of the RR1 dataset with color composites displayed in Fig. 8. Linear stretching between 1% and 99% of the histogram range for each band is used for visualization.

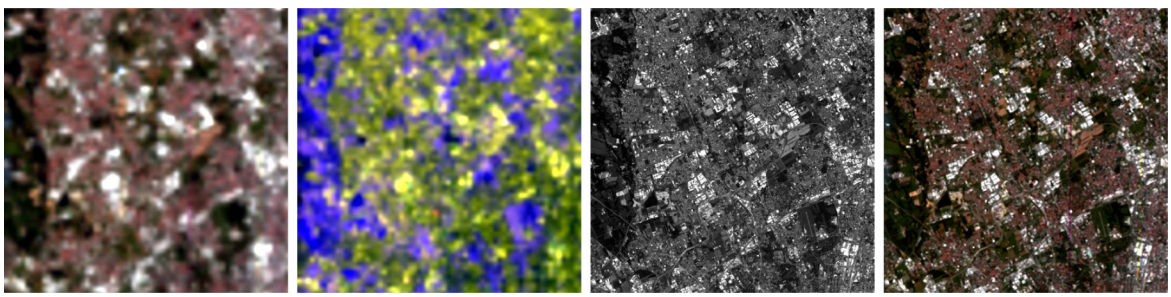

Fig. 10. 400×400 portions of the RR2 dataset. From left to right: Color composites of the HS image degraded at 180 m and resampled at 30 m, true-color (641, 563, 478) nm and false-color (1726, 1575, 855) nm; Pan image degraded at 30 m; true-color original at 30 m (reference, not distributed).

deep networks with millions of parameters working after a lightweight training involving few samples compared to the number of parameters (biases and weights) to estimate. It is worth to remark that the training is an estimation problem where a number of parameters related to the particular network configuration is estimated starting from the available samples (examples) provided during the training phase. Some constraints can sometimes be added to facilitate the training. A classical example is provided by convolutional neural networks (widely exploited for computer vision tasks), which implicitly limit

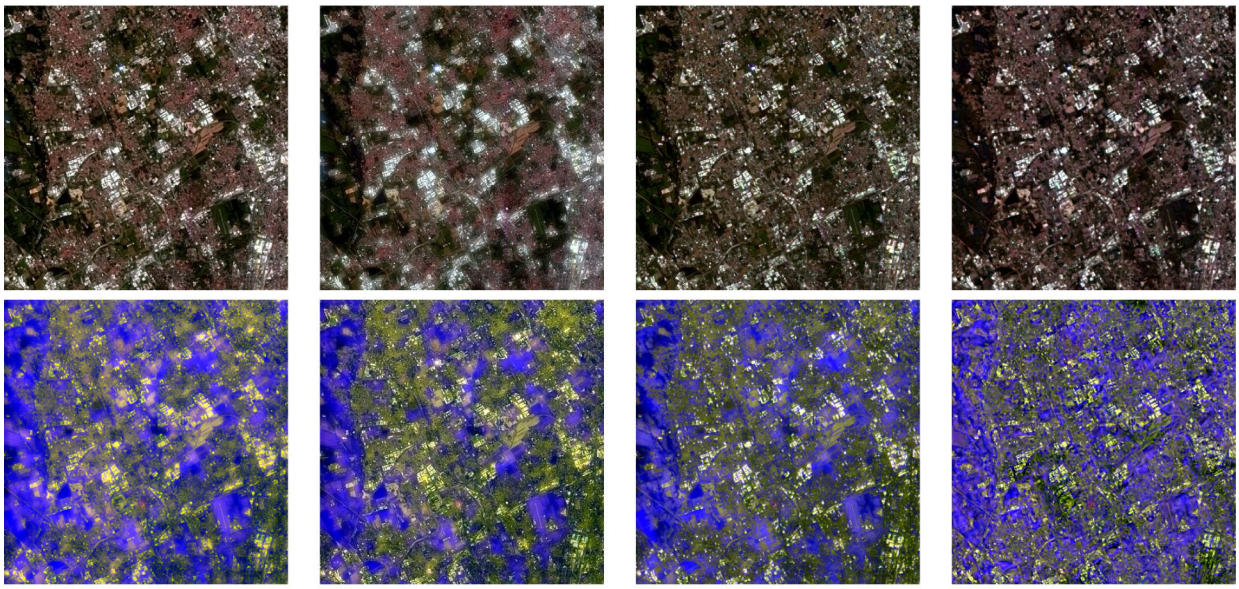

Fig. 11. Pansharpening results on a 400×400 portion of the RR2 dataset with color composites displayed in Fig. 10. Linear stretching between 1% and 99% of the histogram range for each band is used for visualization.

connections to a neighborhood, thus reducing the size of the receptive field with respect to fully connected neural networks. However, to estimate millions of parameters, a huge amount of data is required that are often unavailable for remote sensing image sharpening. Hence, a clear reduction of the training phase, because of the absence of data, leads to the adaptation of neural networks to the particular problem presented in the training phase, thus decreasing their generalization ability. This problem, which is a hot topic for multispectral pansharpening, is still more crucial for hyperspectral sharpening because hundreds of spectral bands are fused with respect to tens of spectral bands of the multispectral case. Indeed, more bands mean more network inputs leading to more complex (with more parameters) networks, thus requiring more data for training.

We want to conclude this section stating that this contest opened our eyes to new problems. The scientific community is moving faster and faster addressing more challenging issues everyday. New potentialities have recently been identified in artificial intelligence solutions for facing with remote sensing image sharpening. Anyway, the Community should also consider the development of remote sensing-based approaches, strongly exploiting knowledge about the problem at hand and integrating it in approaches that are not just borrowed from other scientific communities (as the computer vision one). Indeed, the exchange of information among communities will surely be the key to success for developing new solutions to address more challenging research problems with outstanding performance.

V. Conclusion

This article presented the scientific outcomes of the 2022 Hyperspectral Pansharpening Challenge organized by the 12th IEEE WHISPERS 2022. The article described first the four datasets used for this challenge, even pointing out the data preparation procedures. Afterward, the baseline approaches forming the benchmark have been detailed together with the protocols (both at reduced resolution and full resolution) for performance assessment of participants' outcomes. Finally, quantitative and qualitative results have been shown with some discussions about these latter and some thoughts on the state of the researches in the field of hyperspectral pansharpening and the new trends in image sharpening.

All in all, the organizers observed a good interest (with more than 100 registrations), but just four teams joined it submitting their outcomes. The participants proposed innovative solutions relied upon machine learning and variational optimization-based methodologies. Anyway, despite the use of the state-of-the-art approaches, the teams did not get outstanding results if we compare them with some baseline methods that were proposed tens of years ago in the multispectral pansharpening literature (see, e.g., the GSA and the MTF-GLP). For this reason, the committee decided to close the contest and claim it is inconclusive (no winner).

Acknowledgment

The authors would like to thank Dr. E. Lopinto, Ground Segment and Applications responsible of ASI PRISMA mission, for his precious contribution to data procurement and distribution to the scientific community.

References

[1] L. Loncan et al., "Hyperspectral pansharpening: A review," *IEEE Geosci. Remote Sens. Mag.*, vol. 3, no. 3, pp. 27–46, Sep. 2015.

[2] G. Vivone, R. Restaino, G. Licciardi, M. Dalla Mura, and J. Chanussot, "Multiresolution analysis and component substitution techniques for hyperspectral pansharpening," in *Proc. IEEE Geosci. Remote Sens. Symp.*, 2014, pp. 2649–2652.

[3] S. Baronti, B. Aiazzi, M. Selva, A. Garzelli, and L. Alparone, "A theoretical analysis of the effects of aliasing and misregistration on pansharpened imagery," *IEEE J. Sel. Topics Signal Process.*, vol. 5, no. 3, pp. 446–453, Jun. 2011.

[4] A. Arienzo, L. Alparone, B. Aiazzi, and A. Garzelli, "Automatic fine alignment of multispectral and panchromatic images," in *Proc. IEEE Int. Geosci. Remote Sens. Symp.*, 2020, pp. 228–231.

[5] L. Capobianco, A. Garzelli, F. Nencini, L. Alparone, and S. Baronti, "Spatial enhancement of Hyperion hyperspectral data through ALI panchromatic image," in *Proc. IEEE Int. Geosci. Remote Sens. Symp.*, 2007, pp. 5158–5161.

[6] A. Garzelli, F. Nencini, and L. Capobianco, "Optimal MMSE pan sharpening of very high resolution multispectral images," *IEEE Trans. Geosci. Remote Sens.*, vol. 46, no. 1, pp. 228–236, Jan. 2008.

[7] M. Khan, J. Chanussot, and L. Alparone, "Hyperspectral pansharpening using QNR optimization constraint," in *Proc. 1st Workshop Hyperspectral Image Signal Process.: Evol. Remote Sens.*, 2009, pp. 1–4.

[8] B. Aiazzi, L. Alparone, S. Baronti, A. Garzelli, and M. Selva, "Hyperspectral image fusion," in *ESA Hyperspectral Workshop*2010, Paper no. ESA SP-683.

[9] J. Qu, Y. Li, and W. Dong, "Hyperspectral pansharpening with guided filter," *IEEE Geosci. Remote Sens. Lett.*, vol. 14, no. 11, pp. 2152–2156, Nov. 2017.

[10] Z. Huang, Q. Chen, Y. Shen, Q. Chen, and X. Liu, "An improved variational method for hyperspectral image pansharpening with the constraint of spectral difference minimization," *Int. Arch. Photogramm. Remote Sens. Spatial Inf. Sci.*, vol. XLII-2/W7, pp. 753–760, Sep. 2017.

[11] W. Dong, J. Liang, and S. Xiao, "Saliency analysis and Gaussian mixture model-based detail extraction algorithm for hyperspectral pansharpening," *IEEE Trans. Geosci. Remote Sens.*, vol. 58, no. 8, pp. 5462–5476, Aug. 2020.

[12] L. He, J. Zhu, J. Li, A. Plaza, J. Chanussot, and B. Li, "HyperPNN: Hyperspectral pansharpening via spectrally predictive convolutional neural networks," *IEEE J. Sel. Topics Appl. Earth Observ. Remote Sens.*, vol. 12, no. 8, pp. 3092–3100, Aug. 2019.

[13] Y. Zheng, J. Li, Y. Li, J. Guo, X. Wu, and J. Chanussot, "Hyperspectral pansharpening using deep prior and dual attention residual network," *IEEE Trans. Geosci. Remote Sens.*, vol. 58, no. 11, pp. 8059–8076, Nov. 2020.

[14] L. He, J. Zhu, J. Li, D. Meng, J. Chanussot, and A. Plaza, "Spectral-fidelity convolutional neural networks for hyperspectral pansharpening," *IEEE J. Sel. Topics Appl. Earth Observ. Remote Sens.*, vol. 13, pp. 5898–5914, 2020.

[15] L. He, J. Zhu, J. Li, A. Plaza, J. Chanussot, and Z. Yu, "CNN-based hyperspectral pansharpening with arbitrary resolution," *IEEE Trans. Geosci. Remote Sens.*, vol. 60, 2022, Art. no. 5518821.

[16] L. He, J. Xie, J. Li, A. Plaza, J. Chanussot, and J. Zhu, "Variable subpixel convolution based arbitrary-resolution hyperspectral pansharpening," *IEEE Trans. Geosci. Remote Sens.*, vol. 60, 2022, Art. no. 5534519.

[17] W. G. C. Bandara, J. M. J. Valanarasu, and V. M. Patel, "Hyperspectral pansharpening based on improved deep image prior and residual reconstruction," *IEEE Trans. Geosci. Remote Sens.*, vol. 60, 2022, Art. no. 5520816.

[18] J. Nie, Q. Xu, and J. Pan, "Unsupervised hyperspectral pansharpening by ratio estimation and residual attention network," *IEEE Geosci. Remote Sens. Lett.*, vol. 19, 2022, Art. no. 6007105. [Online]. Available: https://ieeexplore.ieee.org/document/9703344/

[19] J. Qu, S. Hou, W. Dong, S. Xiao, Q. Du, and Y. Li, "A dual-branch detail extraction network for hyperspectral pansharpening," *IEEE Trans. Geosci. Remote Sens.*, vol. 60, 2022, Art. no. 5518413.

[20] P. Guan and E. Y. Lam, "Multistage dual-attention guided fusion network for hyperspectral pansharpening," *IEEE Trans. Geosci. Remote Sens.*, vol. 60, 2022, Art. no. 5515214.

[21] X. Wu, J. Feng, R. Shang, X. Zhang, and L. Jiao, "Multiobjective guided divide-and-conquer network for hyperspectral pansharpening," *IEEE Trans. Geosci. Remote Sens.*, vol. 60, 2022, Art. no. 5525317.

[22] W. Dong, Y. Yang, J. Qu, W. Xie, and Y. Li, "Fusion of hyperspectral and panchromatic images using generative adversarial network and image segmentation," *IEEE Trans. Geosci. Remote Sens.*, vol. 60, 2022, Art. no. 5508413.

[23] W. Dong, T. Zhang, J. Qu, S. Xiao, J. Liang, and Y. Li, "Laplacian pyramid dense network for hyperspectral pansharpening," *IEEE Trans. Geosci. Remote Sens.*, vol. 60, 2022, Art. no. 5507113.

[24] J. Qu, Y. Shi, W. Xie, Y. Li, X. Wu, and Q. Du, "MSSL: Hyperspectral and panchromatic images fusion via multiresolution spatial–spectral feature learning networks," *IEEE Trans. Geosci. Remote Sens.*, vol. 60, 2022, Art. no. 5504113.

[25] M. Kremezi et al., "Pansharpening PRISMA data for marine plastic litter detection using plastic indexes," *IEEE Access*, vol. 9, pp. 61955–61971, 2021.

[26] ASI, "ASI PRISMA Portal," Accessed: Aug. 1, 2022. [Online]. Available: https://prisma.asi.it/

[27] ASI, "PRISMA algorithm theoretical basis document (ATBD)," Accessed: Aug. 1, 2022. [Online]. Available: http://prisma.asi.it/missionselect/docs/PRISMA%20ATBD_v1.pdf

[28] ASI, "PRISMA products specification document," Accessed: Aug. 1, 2022. [Online]. Available: http://prisma.asi.it/missionselect/docs/PRISMA%20Product%20Specifications_Is2_3.pdf

[29] Open Remote Sensing, "Outcome of the 2022 WHISPERS hyperspectral pansharpening challenge." [Online]. Available: https://tinyurl.com/4u2ax8v7

[30] G. Vivone et al., "A new benchmark based on recent advances in multispectral pansharpening: Revisiting pansharpening with classical and emerging pansharpening methods," *IEEE Geosci. Remote Sens. Mag.*, vol. 9, no. 1, pp. 53–81, Mar. 2021.

[31] G. Vivone et al., "A critical comparison among pansharpening algorithms," *IEEE Trans. Geosci. Remote Sens.*, vol. 53, no. 5, pp. 2565–2586, May 2015.

[32] C. A. Laben and B. V. Brower, "Process for enhancing the spatial resolution of multispectral imagery using pan-sharpening," U.S. Patent #6011875, 2000.

[33] B. Aiazzi, S. Baronti, and M. Selva, "Improving component substitution pansharpening through multivariate regression of MS pan data," *IEEE Trans. Geosci. Remote Sens.*, vol. 45, no. 10, pp. 3230–3239, Oct. 2007.

[34] X. Otazu, M. González-Audícana, O. Fors, and J. Núñez, "Introduction of sensor spectral response into image fusion methods. application to wavelet-based methods," *IEEE Trans. Geosci. Remote Sens.*, vol. 43, no. 10, pp. 2376–2385, Oct. 2005.

[35] B. Aiazzi, L. Alparone, S. Baronti, A. Garzelli, and M. Selva, "MTF-tailored multiscale fusion of high-resolution MS and pan imagery," *Photogramm. Eng. Remote Sens.*, vol. 72, no. 5, pp. 591–596, May 2006.

[36] R. Restaino, G. Vivone, M. Dalla Mura, and J. Chanussot, "Fusion of multispectral and panchromatic images based on morphological operators," *IEEE Trans. Image Process.*, vol. 25, no. 6, pp. 2882–2895, Jun. 2016.

[37] G. Vivone, R. Restaino, M. Dalla Mura, G. Licciardi, and J. Chanussot, "Contrast and error-based fusion schemes for multispectral image pansharpening," *IEEE Geosci. Remote Sens. Lett.*, vol. 11, no. 5, pp. 930–934, May 2014.

[38] L. Wald, T. Ranchin, and M. Mangolini, "Fusion of satellite images of different spatial resolutions: Assessing the quality of resulting images," *Photogramm. Eng. Remote Sens.*, vol. 63, no. 6, pp. 691–699, Jun. 1997.

[39] L. Alparone, B. Aiazzi, S. Baronti, A. Garzelli, F. Nencini, and M. Selva, "Multispectral and panchromatic data fusion assessment without reference," *Photogramm. Eng. Remote Sens.*, vol. 74, no. 2, pp. 193–200, Feb. 2008.

[40] R. H. Yuhas, A. F. H. Goetz, and J. W. Boardman, "Discrimination among semi-arid landscape endmembers using the spectral angle mapper (SAM) algorithm," in *Proc. Summaries 3rd Annu. JPL Airborne Geosci. Workshop*, 1992, pp. 147–149.

[41] L. Wald, *Data Fusion: Definitions and Architectures—Fusion of Images of Different Spatial Resolutions*. Paris, France: Les Presses de l'École des Mines, 2002.

[42] A. Garzelli and F. Nencini, "Hypercomplex quality assessment of multi/hyperspectral images," *IEEE Trans. Geosci. Remote Sens.*, vol. 6, no. 4, pp. 662–665, Oct. 2009.

[43] A. Arienzo, G. Vivone, A. Garzelli, L. Alparone, and J. Chanussot, "Full resolution quality assessment of pansharpening: Theoretical and hands-on approaches," *IEEE Geosci. Remote Sens. Mag.*, vol. 10, no. 3, pp. 168–201, Sep. 2022.

[44] L. Alparone, A. Garzelli, and G. Vivone, "Spatial consistency for full-scale assessment of pansharpening," in *Proc. IEEE Int. Geosci. Remote Sens. Symp.*, 2018, pp. 5132–5134.

[45] M. Simoes, J. Bioucas-Dias, L. Almeida, and J. Chanussot, "A convex formulation for hyperspectral image superresolution via subspace-based regularization," *IEEE Trans. Geosci. Remote Sens.*, vol. 53, no. 6, pp. 3373–3388, Jun. 2015.

Gemine Vivone (Senior Member, IEEE) received the B.Sc. (summa cum laude), the M.Sc. (summa cum laude), and the Ph.D. (highest rank) degrees in information engineering from the University of Salerno, Salerno, Italy, in 2008, 2011, and 2014, respectively.

He is a Researcher with the National Research Council (Italy). In 2019, he was an Assistant Professor with the University of Salerno. In 2014, he joined the North Atlantic Treaty Organization (NATO) Science & Technology Organization (STO) Centre for Maritime Research and Experimentation (CMRE), La Spezia, Italy, as a Scientist. In 2019, he was a Visiting Professor with the Grenoble Institute of Technology (INPG), Grenoble, France. His main research interests include statistical signal processing, detection of remotely sensed images, data fusion, and tracking algorithms.

Dr. Vivone is a Co-Chair of the IEEE GRSS Image Analysis and Data Fusion Technical Committee. He was the Leader of the Image and Signal Processing Working Group of the IEEE Image Analysis and Data Fusion Technical Committee (2020–2021). He is currently an Associate Editor for the *IEEE Geoscience and Remote Sensing Letters (GRSL)*, an Editorial Board Member of *Nature Scientific Reports*, *MDPI Remote Sensing*, and *MDPI Sensors*, and an Associate Editor and Reviewer Editor for *Frontiers in Remote Sensing*. He served as Guest Associate Editor for several Special Issues. He was the recipient of the IEEE GRSS Early Career Award in 2021, the Symposium Best Paper Award at IEEE International Geoscience and Remote Sensing Symposium (IGARSS) in 2015, and the Best Reviewer Award of the IEEE TRANSACTIONS ON GEOSCIENCE AND REMOTE SENSING in 2017. Moreover, he is listed in the World's Top 2% Scientists by Stanford University for single-years 2019, 2020, 2021 and for the entire career.

Andrea Garzelli (Senior Member, IEEE) received the 'Laurea' degree (cum laude) in electronic engineering and the Ph.D. degree in computer science and telecommunication engineering (highest rank) from the University of Florence, Florence, Italy, in 1991 and 1995, respectively.

He is an Associate Professor, awarded with research accreditations as Full Professor, with the Department of Information Engineering and Mathematics (DIISM), University of Siena, Siena, Italy. He holds the courses of "Fundamentals of Telecommunications," "Statistical Signal Processing," and "Remote Sensing" at the University of Siena. He is currently the Program Coordinator of the graduate course in Computer and Information Engineering with DIISM. His main research interests include remote sensing image processing from optical and SAR sensors and image fusion.

Dr. Garzelli is listed in the World's Top 2% Scientists by Stanford University for single-years 2021, 2020, 2019, and for the entire career.

Yang Xu (Member, IEEE) received the B.Sc. degree in applied mathematics and the Ph.D. degree in pattern recognition and intelligence systems from the Nanjing University of Science and Technology (NJUST), Nanjing, China, in 2011 and 2016, respectively.

He is currently an Associate Professor with the School of Computer Science and Engineering, NJUST. He was a Visiting Scholar with the GIPSA-lab, Grenoble INP, University of Grenoble Alpes, Grenoble, France, in 2015 and 2018. His research interests include hyperspectral image processing, image fusion, and machine learning.

Dr. Xu serves as an Associate Editor for the *IEEE Geoscience and Remote Sensing Letters*.

Wenzhi Liao (Senior Member, IEEE) received the B.Sc. degree in mathematics from Hainan Normal University, Haikou, China, in 2006, the Ph.D. degree in engineering from the South China University of Technology, Guangzhou, China, in 2012, and the Ph.D. degree in computer science engineering from Ghent University, Ghent, Belgium, in 2012.

From 2012 to 2019, he was a Postdoctoral Research Fellow first with Ghent University and then with the Research Foundation Flanders (FWO), Vlaanderen, Belgium. From February 2020 to January 2022, he has been with the Sustainable Materials Management, Flemish Institute for Technological Research (VITO), Mol, Belgium. Since February 2022, he has been with Flanders Make, focusing on smart vision for Industry 4.0. He is also the Guest Professor with Ghent University. His research interests include image processing, pattern recognition, remote sensing, and material recycling. In particular, his interests include mathematical morphology, multisensor data fusion, hyperspectral image (HSI) restoration, and AI for recycling.

Dr. Liao was a recipient of the Best Paper Challenge Awards in both the 2013 IEEE GRSS Data Fusion Contest and the 2014 IEEE GRSS Data Fusion Contest. He serves as an Associate Editor for the *IEEE Journal of Selected Topics in Applied Earth Observations and Remote Sensing (JSTARS)*.

Jocelyn Chanussot (Fellow, IEEE) received the M.Sc. degree in electrical engineering from the Grenoble Institute of Technology (Grenoble INP), Grenoble, France, in 1995, and the Ph.D. degree from the Université de Savoie, Annecy, France, in 1998.

Since 1999, he has been with Grenoble INP, where he is currently a Professor of signal and image processing. He has been a Visiting Scholar with Stanford University, Stanford, CA, USA, KTH, Stockholm, Sweden, and NUS, Singapore. Since 2013, he has been an Adjunct Professor with the University of Iceland, Reykjavik, Iceland. From 2015 to 2017, he was a Visiting Professor with the University of California, Los Angeles (UCLA), Los Angeles, CA, USA. He holds the AXA chair in remote sensing and is an Adjunct professor at the Chinese Academy of Sciences, Aerospace Information research Institute, Beijing. He has coauthored more than 250 papers in international journals, gathering 31500+ citations, with h index=78. His research interests include image analysis, hyperspectral remote sensing, data fusion, machine learning, and artificial intelligence.

Dr. Chanussot is the founding President of IEEE Geoscience and Remote Sensing French chapter (2007–2010), which received the 2010 IEEE GRS-S Chapter Excellence Award. He is the recipient of multiple outstanding paper awards. He was the Vice-President of the *IEEE Geoscience and Remote Sensing Society*, in charge of meetings and symposia (2017–2019). He was the General Chair of the first IEEE GRSS Workshop on Hyperspectral Image and Signal Processing, Evolution in Remote sensing (WHISPERS). He was the Chair (2009–2011) and Cochair of the GRS Data Fusion Technical Committee (2005–2008). He was a Member of the Machine Learning for Signal Processing Technical Committee of the IEEE Signal Processing Society (2006–2008) and the Program Chair of the IEEE International Workshop on Machine Learning for Signal Processing (2009). He is an Associate Editor for the IEEE TRANSACTIONS ON GEOSCIENCE AND REMOTE SENSING, the IEEE TRANSACTIONS ON IMAGE PROCESSING and the *Proceedings of the IEEE*. He was the Editor-in-Chief for the *IEEE Journal of Selected Topics in Applied Earth Observations and Remote Sensing* (2011–2015). In 2014, he served as a Guest Editor for the IEEE Signal Processing Magazine. He is an ELLIS Fellow, a Fellow of the Asia-Pacific Artificial Intelligence Association, a Member of the Institut Universitaire de France (2012–2017), and a Highly Cited Researcher (Clarivate Analytics/Thomson Reuters, since 2018).